# Doping rich ethylene premixed flames: Influence of C 3 C 5 alcohols on the structure of the steady one-dimensional laminar flame

R. Jalain, J. Bonnety, G. Legros, A. Matynia

## ▶ To cite this version:

HAL Id: hal-03413871

https://hal.science/hal-03413871

# Doping rich ethylene premixed flames: influence of $C_3$-$C_5$ alcohols on the structure of the steady one-dimensional laminar flame

R. Jalain[a,*], J. Bonnety[a], G. Legros[b], A. Matynia[a]

[a]*Sorbonne Université, Centre National de la Recherche Scientifique, UMR 7190, Institut Jean Le Rond d´Alembert, Paris F-75005, France*
[b]*CNRS-ICARE, 1C Avenue de la Recherche Scientifique, 45071 Orléans Cedex 2, France*

**Abstract**

The addition of alcohols to fueled mixture has been extensively documented as a practical way to significantly mitigate soot emissions by internal combustion engines. While being crucial to the initiation of some soot precursors formation, some chemical pathways attributed to the presence of alcohol-derived species remain unclear. Consequently, atmospheric steady flat laminar rich (equivalence ratio $\phi$=1.7) ethylene/air premixed flames were established over a McKenna burner. The unburnt stream was seeded by prevaporized alcohols ranging from $C_3$ to $C_5$. Every flame was probed and sampled gases were investigated using a gas chromatography (GC) device equipped with a flame ionization detector (FID). Thus, quantitative mole fraction profiles are reported as a function of the distance to the burner tip. In total, 17 chemical compounds, including isomeric species (butene and pentene) have been detected quantitatively. Significant discrepancies among the intermediate species pool were observed, especially the amount of propene, butene, and pentene isomers (produced mostly due to the addition of propanol, butanol, and pentanol, respectively). Several kinetic mechanisms support the experimental results, none of them do reproduce properly the alkene production measured. Further numerical investigations were conducted focusing on the pathways that lead to the production of the alkenes identified. To the authors' knowledge, the results reported are the first that (i) provide experimental results for the addition of 2,2-dimethyl-propanol, (ii) document unambiguously the mole fraction profiles of the three butene and five pentene isomers, and (iii) unveil similar trends on alkene production due to the addition of $C_3$ to $C_5$ alcohols, i.e. a clear hierarchy among primary, secondary, and tertiary alcohols for the rich atmospheric premixed flames studied.

*Keywords:* Flame structure, alcohol addition, alcohol isomer, soot precursors

## 1. Introduction

Among the main features of the oxygenated fuels are their ability to reduce the emissions of particulate matter [1, 2, 3, 4, 5] together with their propensity to form toxic byproducts such as aldehydes or ketones [6, 7, 8]. Heavy alcohols, with their isomeric properties, can mitigate both effects, by choosing the correct isomer or mixture. Moreover, they exhibit higher energy content, lower corrosivity, and are less hygroscopic than ethanol, which is widely used in gasoline engines. Interestingly, propanol, butanol, and pentanol can all be produced by microbial processes ([9, 10, 11, 12]) and they are compatible with an utilization as additives to both gasoline and diesel.

While numerous studies have been dedicated to propanol isomers, i.e. 1- and 2-propanol [13, 14, 15, 16, 17, 18, 19], and all the isomers of butanol (namely, 1-butanol, 2-butanol, *i*-butanol/2-methyl-1-propanol, *t*-butanol/ 2-methyl-2-propanol) [6, 20, 21, 7, 22, 23, 24, 25], the literature on pentanol isomers is relatively sparse. Over the four primary alcohol isomers, three, i.e. 1-pentanol, 2-methyl-butanol, and *i*-pentanol/3-methyl-1-butanol, seem to be the most investigated ones ([26, 27, 28, 29, 30, 31]), followed by the secondary alcohols, 2-pentanol and 3-pentanol [32, 8]. In contrast, the only tertiary alcohol isomer, i.e. *t*-pentanol/2-methyl-2-butanol [31], the secondary 3-methyl-2-butanol and the primary 2,2-dimethyl-propanol suffer from an apparent lack of data. For the latter, its solid state below 325 K (at atmospheric pressure) makes it tricky to blend at a controled content to a gaseous stream.

---
[*]Corresponding author:
*Email address:* `renaud.jalain@sorbonne-universite.fr` (R. Jalain)

As a result, kinetic mechanisms have been developed for propanol and butanol isomers, as well as some pentanol isomers. Among others, the CRECK modeling group developed a free-access kinetic mechanism including propanol and butanol [16, 15]. Recently, Li et al. [18] published a mechanism on propanol isomers. Sarathy et al. [4] also delivered a mechanism for the propanol and butanol isomers. Several kinetic mechanisms have been developed for 1-pentanol [28, 27], 2-methyl-1-butanol [33, 30], and *i*-pentanol [26, 4]. Finally, Kölher et al. built a mechanism specifically developed for the three linear pentanol isomers [8].

Throughout the extensive literature on butanol, which includes the three types of alcohols, some characteristics have reached a consensus. For instance, the unstretched laminar flame speed seems to decrease while adding methyl groups, i.e. 1-butanol and *t*-butanol exhibit the highest and lowest speed, respectively [21, 23]. A similar conclusion was drawn for pentanols isomers in Ref. [31]. On the opposite, conclusions about sooting tendencies are more blurry. Most of the studies state that tertiary alcohols generate more hydrocarbon intermediates leading to more soot, while primary and secondary alcohols produce more oxygenated intermediates, preferentially forming aldehydes or ketones [6, 7]. That being said, a recent study unveiled an opposite trend, showing that among the butanol isomers in the specific conditions of the study the highest rate in particulate matter reduction was achieved by *t*-butanol [25].

Within the scope of the current study, the investigations will focus on alkene production by alcohol dopants in rich flames of a well-studied sooting fuel, i.e. $C_2H_4$, which might the soot production pathways. As detailed in Sarathy's review Alcohol combustion chemistry [4], two major ways of alkene production can be identified.

Firstly, at high temperatures (above 1500 K) and in fuel-rich conditions, the consumption of alcohols is dominated by unimolecular decomposition. Such reactions are important for correctly simulating soot emissions, and non-premixed diffusion flame structures. In all alcohols, these reactions consist of simple C-C and C-H bond scission reactions. Unimolecular water elimination (i.e. dehydration) reactions are also important for alcohols. The four-center reactions involving the $\beta$ hydrogen atoms are the most thermodynamically favored and result in the formation of an alkene and water (R1).

$$C_xH_yOH \rightleftharpoons C_xH_{y-1} + H_2O \qquad (R1)$$
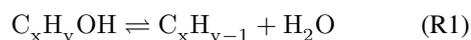
The reaction rate coefficients of four-center dehydration reactions vary with the extent of substitution be-
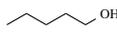
cause this affects the number of abstractable $\beta$ hydrogen atoms and their bond dissociation energies (i.e., primary, secondary, or tertiary).

Secondly, fuel radicals can undergo unimolecular decomposition via $\beta$-scission at relatively high temperatures (e.g., 900 K). In these reactions, the bonds located in the $\beta$ position of the radical carbon are weakened and break to form an unsaturated species and another radical. $\beta$-scission of C-C and C-H bonds leads to the formation of unsaturated alcohols or alkenes (i.e. C=C bonds, reaction R2), whereas $\beta$-scission of the O-H bonds results in the formation of a carbonyl group (i.e. C=O bond).

$$\cdot C_xH_{y-1}OH \rightleftharpoons C_xH_{y-1} + \cdot OH \qquad (R2)$$
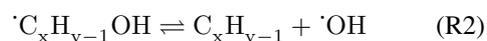
The present work intends to characterize the intermediate hydrocarbons production attributed to each of the $C_3$ to $C_5$ alcohols (cf. Tab. 1) when it seeds the unburnt $C_2H_4$/air stream of an atmospheric laminar flat premixed flame. The set of experiments especially leads to the measurements of the mole fraction profiles of $C_1$ to $C_5$ hydrocarbons, with isomeric separation of butene and pentene.

Table 1: Nomenclature of studied alcohols.



| 1-propanol | 2-propanol | | |
| 1-butanol | 2-butanol | *i*-butanol | *t*-butanol |
| 1-pentanol | 2-pentanol | *i*-pentanol | *t*-pentanol |
| 2-methyl-1-butanol | 3-pentanol | 3-methyl-2-butanol | 2,2-dimethyl-1-propanol |

## 2. Experimental setup

### 2.1. Flames and burner

A rich flat flame ($\phi$=1.7) of ethylene/air established over a McKenna burner at atmospheric pressure is seeded by a single additive, selected among the different isomers of propanol, butanol, and pentanol (cf. Fig. 1). The experimental parameters are reported in Tab. 2. A base flame of pure ethylene with a flowrate of 0.984 nl/min is also investigated.

As extensively outlined in Ref. [34], the liquid additive is to be prevaporized, then blended at a controlled content with the flow of ethylene which is here the carrier gas. The liquid flow rate is adjusted by a Bronkhorst Cori-Flow mass flow controller while a Bronkhorst EL-Flow one regulates the ethylene flow rate. The liquid additive is evaporated and mixed with ethylene in a CEM (Controlled Evaporator Mixer). The liquid fuel flow is set to get 3.5 % (in mole) of vapor $\left(X_{\text{vap}}\right)$ in the carrier gas. Connected to the outlet of the CEM, a heated line (referred to as HL in the following) feeds the burner with the unburnt gaseous mixture. A second heated line supplies the burner with air, the flow of which is regulated by a second Bronkhorst EL-Flow mass flow controller. The total mass flow rate is set to 12 g/min. A nitrogen shield flows around the burner to prevent any perturbation from the environment. A water circuit inside the burner allows to regulate the temperature of the porous section. The regulation is ensured by a heating cartridge as hot source and fans as cold source.

To further improve the flame stability, especially for rich flames, a disk of non coated cellular monolith ceramic is held at 1 cm above the burner output (see Fig.1 c)). The ceramic disk is meshed by 600 cells per square inch to allow the circulation of burnt gases and limit the upstream propagation of the local perturbations.

To compare the behaviour of different fuels, experimenters have to choose which content to be held constant. There are several options such as exit velocity [35], volume fraction [36], molar fraction [37, 34, 38] or total carbon mass [39]. Each one has side effects, (i) constant exit velocity and constant volume fraction might be unadvised if the range of fuel densities is important, (ii) molar fraction might be unadvised if the range of fuels number of carbon is important, (iii) total mass carbon might be unadvised for molecules containing atoms different from carbon and hydrogen. For instance by keeping the total carbon mass constant for propanol and pentanol would lead to add more oxygen in the case of propanol than pentanol, thus improving the oxydative potential of the mixture, which could, for instance, lead to shift the balance regarding sooting tendency of the dopants. Usually in the case of dopant, the amount staying low, the base flame must not be too affected, therefore the choice might not impact the tendencies too much. Moreover if the experimental result are supported by numerical simulations the impact will be taken into account.

In the current paper, the liquid fuel flow has been set to 3.5 % (in mole) of vapor $\left(X_{\text{vap}}\right)$. This amount is expected to not change significantly the ethylene flame

properties (such as temperature and thickness) and allows to control the alcohol flow properly and to measure significantly the discrepancies among the isomers. Constant molar fraction has been chosen to keep the same quantity of matter into the combustion. Propanol, butanol and pentanol having different molecular weights, mass flow had to be modified to keep the molecular amount constant.

Table 2: Premixed flame parameter values.

| Parameter | | | Value | |
|---|---|---|---|---|
| CEM (K) | | | 353 | ±2 |
| HL (K) | | | 323 | ±5 |
| Burner (K) | | | 323 | ±2 |
| $\phi$ | | | 1.70 | ± 0.04 |
| $X_{\text{vap}}$ | | | 0.035 | $\pm 4.10^{-4}$ |
| $N_2$ (nl/min) | | | 9.00 | ±0.12 |
| Air (nl/min) | | | 8.30 | ±0.11 |
| | prop. | but. | pent. | |
| $C_2H_4$ (nl/min) | 0.931 | 0.915 | 0.900 | ±0.011 |
| Alcohol (g/h) | 5.47 | 6.64 | 7.76 | ±0.04 |

## 2.2. Sampling and analysis

Gaseous sampling was performed along the vertical axis $z$ at different heights above the burner (HAB) with a quartz probe, connected to a vacuum pump, and stored in spherical glass flasks (volume V=1 l). The quartz probe orifice is about 60 μm diameter. Flasks are vacuumed before each experiment and then filled by the sampled gas up to 4 kPa. A sampling can be done by step of 100 μm along the vertical axis $z$ of the flame by moving the burner downwards with a stepper motor. The samples are then injected into a Gas Chromatography device (GC) equipped with a Flame Ionization Detector (FID). To this end, the gas to be analyzed is transferred in a compression vessel connected to a sample loop of 200 μl and a piston is used to adjust the pressure to 20 kPa before the injection into the Varian 4000 GC/MS.

The relatively small diameter of the probe orifice allows minimizing the sampling volume (and therefore the potential shift between the burner and the sampling position) together with the flow perturbations. A pressure level of 20 kPa has been set after having characterized a linear response between the injection pressure and the FID response, to maximize the FID response while keeping a reasonable time to achieve the samples. In addition, a level of 4 kPa has been selected to have an appropriate quantity of gas to be injected into the
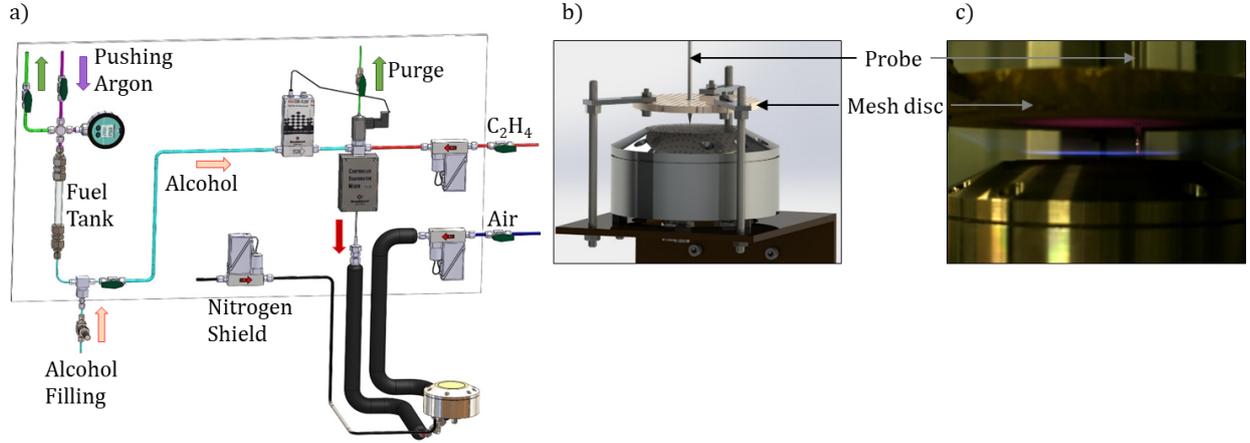
Figure 1: Experimental setup: a) Burner alimentation; b) 3D view of the burner with sampling probe and ceramic mesh disc; c) Picture of the flame on the McKenna burner.

GC/MS at the required pressure. It is worth mentioning that filling a flask requires between 2.25 and 3.5 minutes depending on the position into the flame.

$C_1$ to $C_5$ hydrocarbons were analyzed by GC/MS with a Restek Rt-Alumina BOND/MAPD separation column. At the exit of the column, a mass spectrometer (MS) enables the identification of unknown peaks and quantitative measurements are provided by FID. This column does not separate alcohol species. Typical chromatograms, the identified species and their order of elution in the Restek Rt-Alumina BOND/MAPD Column are available in the supplementary material.

### 2.3. Molar fraction profiles

Two calibration methods have been used to calibrate the GC/MS measurements. First, a standard bottle was used to link the peak areas to the molar fractions of 8 species (cf. Table 3) by the relation :

$$X_i = \frac{A_i}{A_i^{std}} X_i^{std} \tag{1}$$

with $X_i$ the sample molar fraction, $A_i$ the sample peak area, $A_i^{std}$ the standard peak area and $X_i^{std}$ the standard molar fraction of the species $i$.

Concerning the species absent from the standard bottle (propadiene, butene isomers and pentene isomers), FID Response Factors (referred as to RF) were used. A. Tipler, from PerkinElmer, published in an Application Note [40] a chromatogram (obtained with a FID) including all the species presented in the current paper. From this chromatogram, where species molar fractions were

| Species | Molar fraction | |
|---|---|---|
| Methane | 1000 ppm | ± 20 |
| Ethane | 1000 ppm | ± 20 |
| Ethylene | 1000 ppm | ± 20 |
| Propane | 200 ppm | ± 4 |
| Propene | 200 ppm | ± 6 |
| Acetylene | 1000 ppm | ± 20 |
| n-Butane | 100 ppm | ± 2 |
| 1,3-Butadiene | 100 ppm | ± 3 |

Table 3: Standard molar fractions provided by *AirLiquide* company.

known, it was possible to compute absolute response factor $RF^{abs}$:

$$RF_i^{abs} = \frac{A_i}{X_i} \tag{2}$$

with $A_i$ the area of the $i$th species $(V \cdot s)$ and $X_i$ the mole fraction (%). Then, the relative response factors were defined between a reference species $ref$ (here 1,3-butadiene), and each of the species $i$ to be calibrated:

$$RF_i^{rel} = \frac{RF_i^{abs}}{RF_{ref}^{abs}} \tag{3}$$

Finally, the molar fraction were computed from the relation:

$$X_i = \frac{1}{RF_i^{rel}} \left( \frac{A_i}{A_{ref}^{std}} X_{ref}^{std} \right) \tag{4}$$

These calculations are presented on Tab. 4. The reference species 1,3-butadiene has been selected because

(i) its FID response was very stable and (ii) most of the species absent from the standard bottle has a $RF^{rel}$ rather close to 1. To evaluate the validity of the method, the molar fraction of the standard ($X^{std}$) were computed by this method. The last column ($X^{std}$) shows the molar fraction of the species present in the standard bottle calculated from the RF method. The maximal differences between the reference values (see Tab. 3) and the calculated values are 12 % (propene and n-butane).

Table 4: FID Response Factor.
The last column ($X^{std}$) shows the molar fraction of the species present in the standard bottle (Tab. 3) calculated from the RF method.

| Species | Extracted for Ref. [40] | | Eq. 2 | Eq. 3 | Eq. 4 |
|---|---|---|---|---|---|
| | X (%) | A ($\mu$V.s) | $RF^{abs}$ ($\mu$V.s/%) | $RF^{rel}$ | $X^{std}$ |
| Ethylene | 2.0025 | 187178 | 93472 | 0.51 | 1055 |
| Ethane | 4.0021 | 398308 | 99525 | 0.54 | 1003 |
| Propane | 6.0185 | 877739 | 145840 | 0.80 | 216 |
| Propene | 3.0038 | 421959 | 140475 | 0.77 | 224 |
| Propadiene | 0.997 | 127910 | 128295 | 0.70 | - |
| n-Butane | 3.9993 | 750601 | 187683 | 1.03 | 112 |
| 1-Butene | 1.9998 | 368216 | 184126 | 1.01 | - |
| *i*-Butene | 1.0025 | 175064 | 174627 | 0.96 | - |
| *trans*-2-Butene | 3.0061 | 548315 | 182401 | 1.00 | - |
| *cis*-2-Butene | 1.9996 | 358177 | 179124 | 0.98 | - |
| 1,3-Butadiene* | 3.0107 | 550241 | 182762 | 1.00 | 100 |
| 1-Pentene | 0.4007 | 82292 | 205371 | 1.12 | - |
| *trans*-2-Pentene | 0.1996 | 41556 | 208246 | 1.14 | - |
| *cis*-2-Pentene | 0.4001 | 82919 | 207246 | 1.13 | - |
| 2-m-2-Butene | 0.1998 | 39758 | 198989 | 1.09 | - |
| 3-m-1-Butene** | Absent | - | 198989 | 1.09 | - |
| 2-m-1-Butene** | Absent | - | 198989 | 1.09 | - |

*Reference species
**Response factor assumed to be equivalent to 2-m-2-Butene

By these two methods, 17 chemical compounds have been identified and quantified. Profiles were realized between a HAB of 0.2 mm and 2 mm. The distance between these two points will be referred as to Z (i.e. 1.8 mm) and will be used in the next sections.

To ensure the robustness of the flame analysis, each profile is the combination of at least two flame profiles (same flame generated twice), realized in two consecutive days (except the 2,2-dimethyl-propanol due to the complexity of the experiment). Points spaced by only 100 μm are always from two different profiles, i.e. two different sets of measurements. Also, realizing a whole profile requires around one hour and during this time the content of alcohol dopant is stable and the vaporization complete.

## 3. Modeling

### 3.1. Simulation parameters

Experimental data were compared to simulations realized with CANTERA [41] software and the *burner flame* configuration with mixture-averaged molecular diffusion and the resolution of the energy equation.

Reaction mechanisms used in the present study are summarized in Tab. 5 and Tab. 6 presents the input conditions used for all the simulations.

Table 5: Utilization of the different kinetic mechanisms

| Mechanism | Propanol 1-, 2- | Butanol 1-, 2-, *i*-, *t*- | Pentanol 1-, 2-, 3- |
|---|---|---|---|
| Li et al. [18] | X | | |
| CRECK [15, 16] | X | X | |
| Sarathy et al. [4] | X | X | |
| Köhler et al. [8] | | | X |

Table 6: Premixed flame parameter values.

| Input | Value | | | Unit |
|---|---|---|---|---|
| $\Phi$ | | 1.70 | | - |
| $P$ | | 1.0 | | bar |
| $T$ | | 323 | | K |
| $\dot{m}$ | | 0.07 | | kg/m$^2$ |
| | prop. | but. | pent. | |
| $X_{alcohol}$ | 0.367 | 0.361 | 0.356 | % |
| $X_{C_2H_4}$ | 10.1 | 9.96 | 9.81 | % |
| $X_{N_2}$ | 70.7 | 70.8 | 70.9 | % |
| $X_{O_2}$ | 18.8 | 18.8 | 18.8 | % |

Because there is no temperature measurement, this latter has been computed by solving the energy equation. As the concentration of additive remains quite low, there are small differences in the temperature profiles among all the flames. The downstream temperature ($z = 5$ cm) for each simulation ranges from 1723 to 1743 K.It is worth mentioning that the *burner flame* model, when the mass flow term is provided, estimates the heat losses to solve the energy equation. By comparison, the mass flow rate and flame temperature obtained for simulations of perfectly adiabatic flames (*free flame* model) are 0.342 kg/s/m$^2$ and 2068 K, respectively. Besides, the flames studied in the present work do not emit yellow/orange light, therefore soot radiative heat losses are likely to be negligible. That being said, it is important to verify how much a wrong estimation of the heat losses may change the analyses and the conclusions established in this paper.

In order to investigate the impact of temperature profile on species concentration profiles, complementary simulations were conducted with imposed temperature profiles (i.e. without resolution of the energy equation). The four alternative profiles tested are shown in Fig. 2. For two of them, the flame thickness is preserved while the maximum temperature reached at the end of combustion is increased by 10% ($\approx$ 170 K) to assess a bad
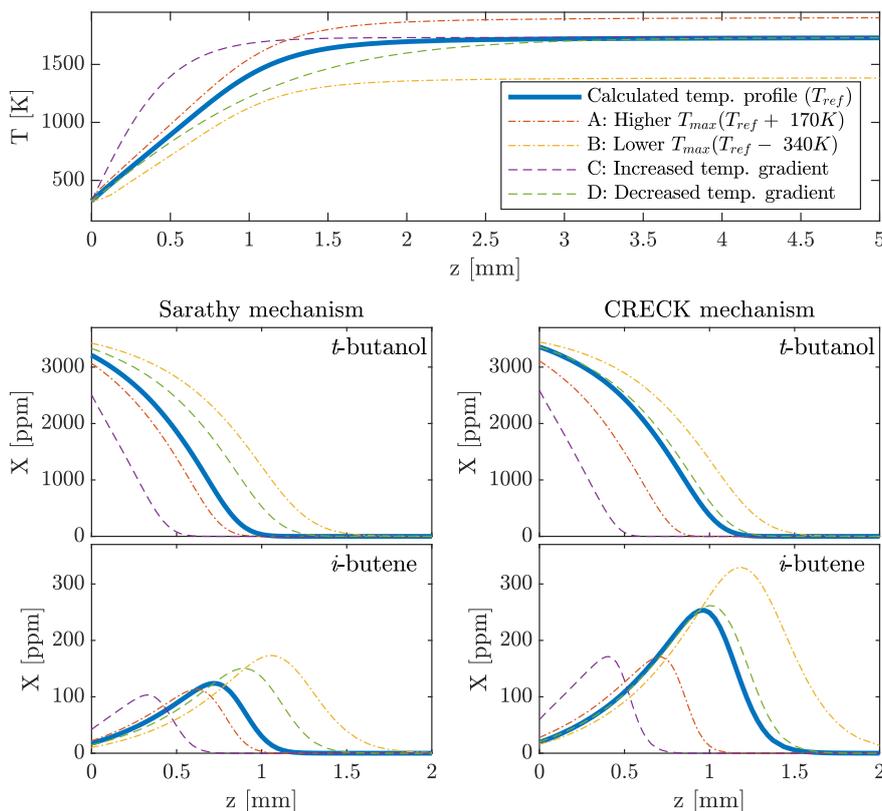
Figure 2: Temperature, *t*-butanol and *i*-butene profiles used to investigate the impact on simulation results

evaluation of the temperature or decreased by 20% to take into account probable heat losses ($\approx 340$ K, see profiles A and B, respectively). The two other profiles have more/less pronounced temperature gradients and the flame thickness is therefore decreased/increased (see profiles C and D, respectively). In spite of these important modifications, the results showed that the maximum molar fraction of studied species never exceeds a factor 1.5 with the reference temperature profile and the observed qualitative trends never change.

### 3.2. Propanol and butanol

Flames doped by propanol isomers were computed by CRECK [15, 16], Li et al. [18] and Sarathy et al. [4] mechanisms. Flames doped by butanol isomers were also computed by CRECK and Sarathy et al. mechanisms.

CRECK mechanism has been developed to simulate the combustion blends of toluene primary reference fuel and alcohols. The mechanism contains 254 species and 7568 reactions. Concerning the propanol isomers, the validation of the kinetic mechanism relies, among others, on structures of counterflow non-premixed flames

and previously reported data over a wide range of configurations and conditions. The model has also been validated by comparing simulations made using this kinetic model with previous and new experimental data on counterflow non-premixed flames of *n*-butanol and *i*-butanol. The structures of these flames were measured by gas sampling from the flame and analyzed by gas chromatography.

Li et al. mechanism contains 156 species and 1413 reactions. The kinetic model of propanol isomers was developed and validated against the experimental data of the paper (flow reactor pyrolysis and laminar flame propagation), as well as other experimental data in literature covering wide ranges of temperatures, pressures and equivalence ratios.

Sarathy et al. mechanism contains 354 species and 2625 reactions and includes detailed high-temperature and low-temperature reaction pathways with reaction rates assigned to describe the unique oxidation features of linear and branched alcohols. Experimental validation targets for the model include low pressure premixed flat flame structure, fundamental laminar flame speeds, rapid compression machine and shock tube ignition de-

lay, and jet-stirred reactor species profiles. The agreement with these various data sets spanning a wide range of temperatures and pressures is reasonably good.

The idea behind confronting several models is to find out where there is room for improvement and where it might have consensus.

### 3.3. Pentanol

To the authors' knowledge there is no mechanism including all isomers, therefore a single mechanism including the three linear ones has been used. Indeed, comparing numerical and experimental results for 8 isomers and adding more models could make the paper reading too tedious.

Simulation of pentanol isomers is realized thanks to the Köhler et al. mechanism (225 species, 24 526 reactions) [8], developed for the combustion of the three linear isomers of pentanol. This kinetic mechanism was built thanks to the open-source software RMG [42], based on the $C_1$-$C_4$ USC mechanism [43] ("seed mechanism" given on RMG) and tested on low pressure $H_2/O_2/Ar$ flames doped by pentanol isomers.

## 4. Results

### 4.1. Overall results

In the present study, all flames are composed of 96.5 % of ethylene and 3.5 % of alcohol isomer. Therefore, temperature and main species molar fractions are likely driven by ethylene combustion rather than the dopants. To support this statement the molar fraction profiles of four species, i.e. $C_2H_4$ (the main fuel), $CH_4, C_2H_6$, and $C_3H_8$, are presented in Fig. 3. For the sake of clarity, the error range, estimated at ±20 %, is displayed at $z$=1 mm for the minimum value in gray and for the maximum value in black. By this way the maximum error of the whole set of experiment is displayed, one can see that for the species presented (considered unaffected by the dopants), there is always a common part between both error ranges.

With 17 species measured for 14 dopants, the experimental data consists in 238 profiles (17 × 14). To simplify the comparisons, the average molar fractions along $Z$ have been computed by the following equation:
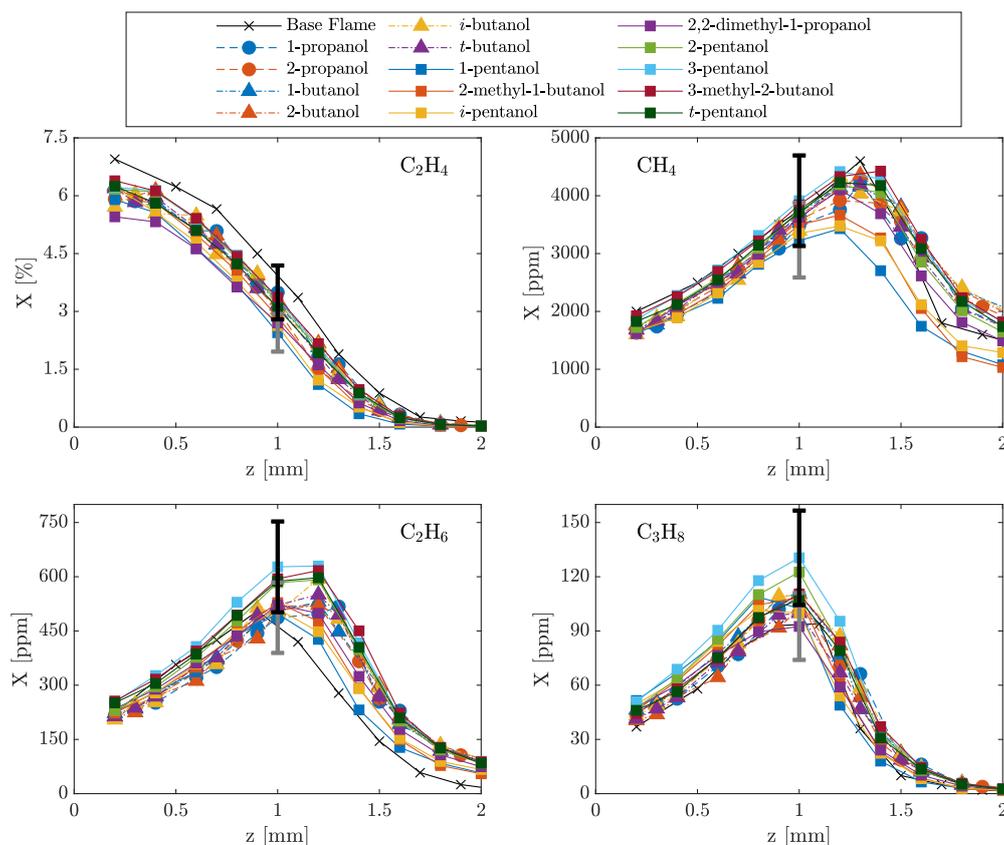


Figure 3: Ethylene, methane, ethane and propane molar fractions profiles.

$$\overline{X}_i = \frac{1}{Z} \int_{0.2}^{2} X_i(z) dz \qquad (5)$$

This method allows mostly to obtain one single value by profile and eventually to encompass noisy data and larger peaks.

Every average molar fraction $\overline{X}_i$ for every dopants are displayed on Fig. 5. The logarithmic $y$-axis scale allows to point out the similarities and discrepancies among the species. For instance, as already mentioned, $C_2H_4$, $CH_4$, $C_2H_6$, $C_3H_8$ but also $C_2H_2$ and $C_4H_{10}$ levels are not influenced by the different dopants. This figure will be referred to numerous times in the following sections. All profiles are available in the supplementary material.

### 4.2. Propanol

Propanol is the smallest alcohol presenting an isomeric structure. The two isomers are the primary alcohol 1-propanol and secondary alcohol 2-propanol. Flame structure analysis revealed that among all the intermediate species measured, only $C_3H_6$ molar fraction profile significantly differs when 1-propanol or 2-propanol are added to ethylene flames.

Figure 4 presents the profiles measured for each of the two flames, as well as, the $\overline{X}$ (eq. 5), representing the average level of the species along $z$. It can be noted that the molar fractions of $C_3H_6$ are almost twice as high for the flames doped with 2-propanol. Similar trends
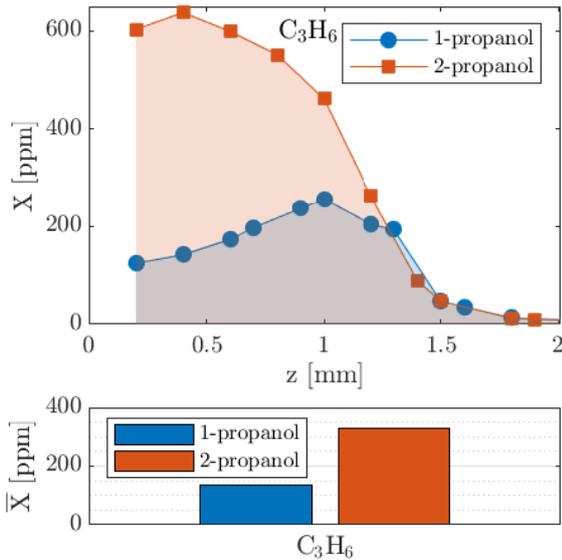


Figure 4: $C_3H_6$ profiles and $\overline{X}$ for 1- and 2-propanol flames.

were obtained in the study by Li et al. [13] who investigated rich ($\phi$=1.8) propanol/$O_2$/Ar premixed flames at 4 kPa. Peak molar fraction measured were then 250 and 390 ppm for 1-propanol and 2-propanol, respectively. A second important aspect of the curve, in the case of 2-propanol, is that the maximum molar fraction is obtained for a much lower $z$, suggesting production reactions starting earlier.

Finally, contrary to the 2-propanol flame, the molar fraction of propene measured in the 1-propanol-doped flame is similar to the ones measured in the base flame and the butanol and pentanol flames (maximum value and location), suggesting that the origin of propene for this flame is mainly driven by the chemical decomposition of ethylene.

Tab. 7 presents the experimental and numerical mean molar fraction of propene. The agreement between experimental and simulated profiles of $C_3H_6$ is acceptable for 1-propanol doped flames (differences of mean molar fractions of about 30 %) given the measurement uncertainties. However, the highest molar fraction of propene observed in 2-propanol doped flames is not reproduced by the simulation, indicating that a pathway toward propene production might be missing or underestimated. Note that the "early" peak location of the propene is not reproduced either.

Propene being a small molecule, there are numerous ways to obtain it. Thus trying to explain this discrepancy seems difficult. However, 2-propanol has two carbons in $\beta$ position from OH, whereas 1-propanol only one. Consequently dehydration (R1) and $\beta$-scission (R2) reactions are more likely to happen. McEnally et al. [6], for instance, attributed the consumption of 1-butanol by dehydration (R1) at 1% against 28% for 2-butanol in $CH_4$ diffusion flame doped with 3500 ppm of butanol.

Table 7: Experimental and numerical level of $\overline{X}_{C_3H_6}$.

| Isomer | Exp. | Li | CRECK | Sarathy |
|---|---|---|---|---|
| 1-propanol | 136 | 95 | 105 | 114 |
| 2-propanol | 327 | 108 | 95 | 125 |

### 4.3. Butanol

Butanol is the smallest alcohol presenting a tertiary alcohol (solid below 300 K), and two primary alcohols. Flame structure analysis of butanol doped flames revealed no significant differences on the molar fraction profiles of $C_1$ and $C_2$ species, as well as propane (cf. Fig. 5). On the contrary, propene, propadiene ($C_3H_4$),
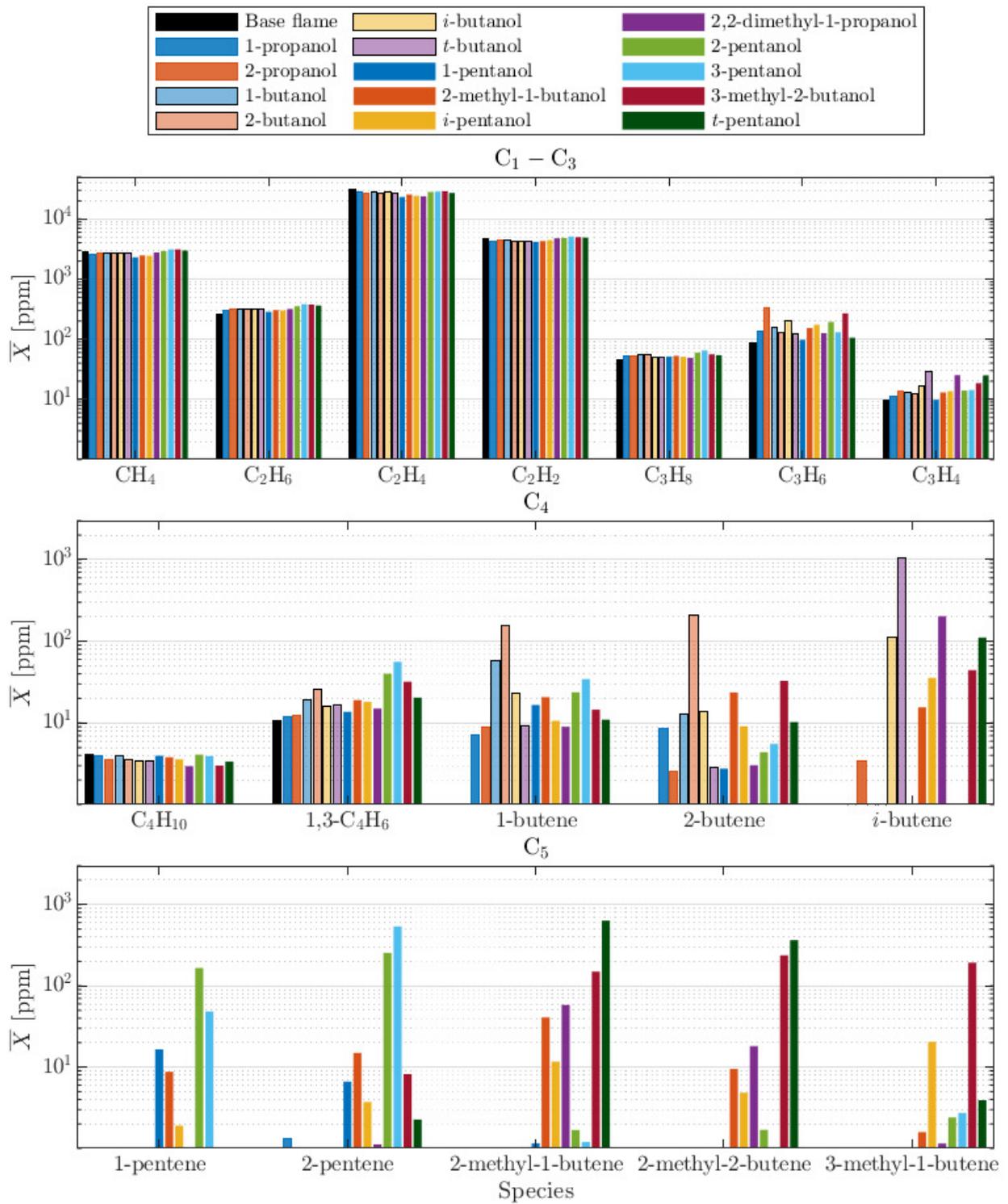
Figure 5: Overall experimental results: $\overline{X}$ of each dopant and each measured species.

butadiene ($C_4H_6$) and butene isomers molar fractions vary depending on the butanol isomer. The maximum molar fraction of propene is observed in *i*-butanol doped flames. The minimum molar fraction is observed, at equivalent levels, for the 2-butanol and *t*-butanol doped flames. On the other hand, propadiene molar fraction is maximum for *t*-butanol then quite similar for the three other isomers (level differences being close to the detection limit). Butadiene molar fraction is maximum for 2-butanol followed by 1-butanol and then the other two isomers. Finally, concerning the butene, the experimental setup allows distinguishing the three isomers. Maximum peak locations are located in the flame, for all cases, earlier than other intermediates (such as the propene profile of the 2-propanol flame).

Because of this early reactivity, reactions like R1 and R2, providing the most direct reaction paths to get butene from butanol, may play an important role. Fig. 6 presents these reactions applied to butanol isomers. In the case of *β*-scission, the first step (H-abstraction on *β* carbon) is not represented.
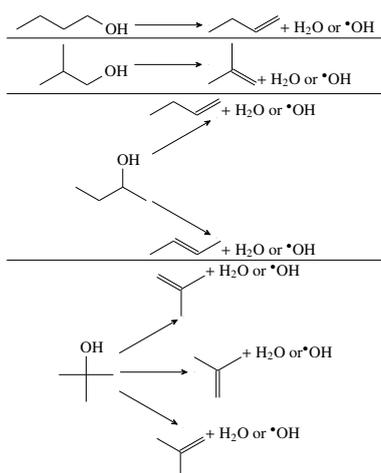


Figure 6: Butanol to butene potential pathways in high-temperature rich-flame.

Butene isomer molar fraction profiles and mean molar fractions are presented in Fig. 7. Observed trends, which can be linked with the aforementioned reaction types, are the following:

1. the major isomer produced in 1-butanol flame is 1-butene and the butene production is much lower than to other blends,
2. *i*-butanol mostly produces *i*-butene,
3. butene isomers produced in 2-butanol doped flames are mostly 1- and 2-butene. Molar fraction levels are quite similar (156 and 207 ppm on average, respectively),

4. *i*-butene is produced almost exclusively in *t*-butanol doped flames and in a high amount compared to other isomers in butanol doped flames.

Interestingly, Oßwald et al. [7] measured mole fraction profiles of butene (without distinctions between isomers) in low-pressure rich ($\phi$=1.7) premixed flames of butanol/$O_2$/Ar and also found a much higher molar fraction in *t*-butanol flames. McEnally et al., in Ref. [6], attributed the consumption of *t*-butanol by dehydration (R1) at 87%.

Tab. 8 provides a comparison between experimental measurements and numerical calculations of averaged butene molar fractions. For ease of reading, the molar fractions of butene isomers are summed.

Table 8: Experimental and numerical level of $\overline{X}_{C_4H_8}$.

| Isomer | Exp. | Sarathy | CRECK |
|---|---|---|---|
| 1-butanol | 71 | 23 | 16 |
| *i*-butanol | 148 | 27 | 34 |
| 2-butanol | 364 | 31 | 14 |
| *t*-butanol | 1065 | 52 | 75 |

Both models compute higher molar fractions of butene in *t*-butanol-doped flame. However, no other similarities are found between experimental and numerical results. Models underestimate butene molar fractions in all cases. Moreover, contrary to experimental observations, there are no significant differences in butene molar fractions between 1-butanol and 2-butanol doped flames. As observed for propanol flames, it seems that the mechanisms do not correctly reproduce the reactivity of alkenes.

### 4.4. Butene isomers production by kinetic mechanisms

This subsection reports which reactions account the most in the production of butene isomers by butanol isomers, and then compare both mechanisms. This aside on specific reactions of kinetic mechanisms focuses on butanol for several reasons: (i) 2 kinetic mechanisms are available, (ii) butanol isomers include the 3 alcohol types, and (iii) there are 3 butene isomers which remains a reasonable number of species to study.

The rate of progress variable $q_i$ for the *i*th reaction is given by the difference of the forward and reverse rates as:

$$q_i = k_{f_i} \prod_{n=1}^{N} [X_n]^{\nu'_{n,i}} - k_{r_i} \prod_{n=1}^{N} [X_n]^{\nu''_{n,i}} \tag{6}$$
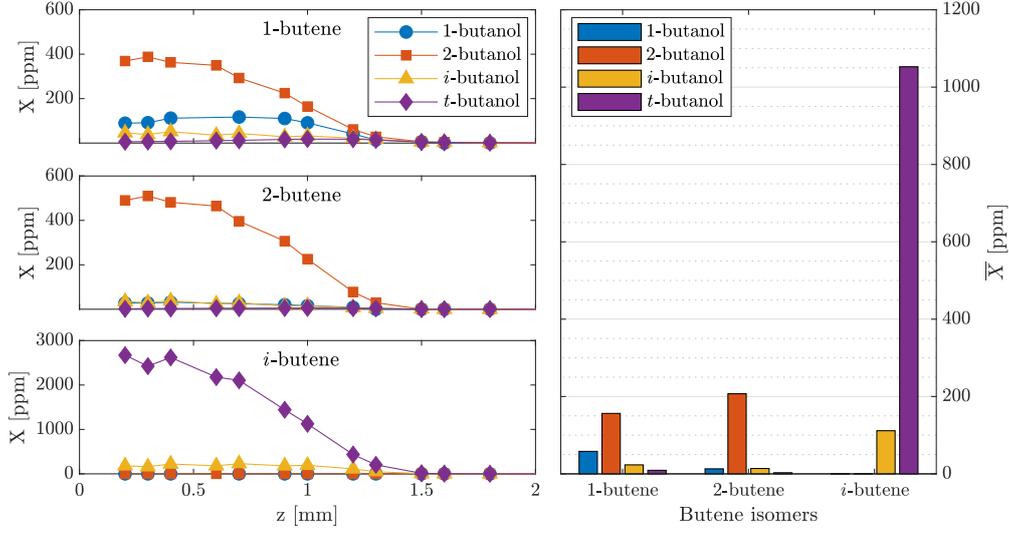
10

Figure 7: Left : Butene isomers profiles ; Right : $\overline{X}$ of butene isomers.

where $[X_n]$ is the concentration of the $n$th species and $k_{f_i}$ and $k_{r_i}$ are the forward and reverse rate constants of the $i$th reaction (given by the mechanism).

Then, the production rate $\dot{\omega}_n$ of the $n$th species can be written as a summation of the rate-of-progress variables for all reactions involving the $n$th species:

$$\dot{\omega}_n = \sum_{i=1}^{I} \nu_{n,i} q_i \qquad (7)$$

where

$$\nu_{n,i} = \nu''_{n,i} - \nu'_{n,i} \qquad (8)$$

with $\nu''_{n,i}$ the reverse stoichiometric coefficients and $\nu'_{n,i}$ the forward stoichiometric coefficients of the $n$th species in the $i$th reaction and $I$ the number of reaction involving the $n$th species.

Hence, computing $\nu_{n,i} q_i$ (referred as to $\dot{\omega}_{n,i}$) for the $I$ reactions involving the $n$th species allows to evaluate the contribution of the $i$th reaction on the production rate. A positive value of $\dot{\omega}_{n,i}$ corresponds to the production of the $n$th species and negative value to its consumption.

To illustrate the methodology, Fig. 8 displays the partial production rates of $t$-butene profile for $t$-butanol flame modeled by CRECK mechanism. Three reactions are responsible of most of the $i$-butene production: dehydration (R1), $\beta$-scission (R2) and H-addition on butenyl. For the sake of readability, only the 10 most contributive reactions are displayed.

The determination of the contribution of $i$th reaction on the production of the $n$th species requires three steps.

Firstly, the reaction rate $\dot{\omega}_{n,i}$ is integrated over $z$ when $\dot{\omega}_{n,i} > 0$ :

$$A_i^{prod} = \int_0^Z \dot{\omega}_{n,i}(z)dz \qquad (9)$$

Secondly, the overall production of this species is calculated by summing the terms for each reaction:
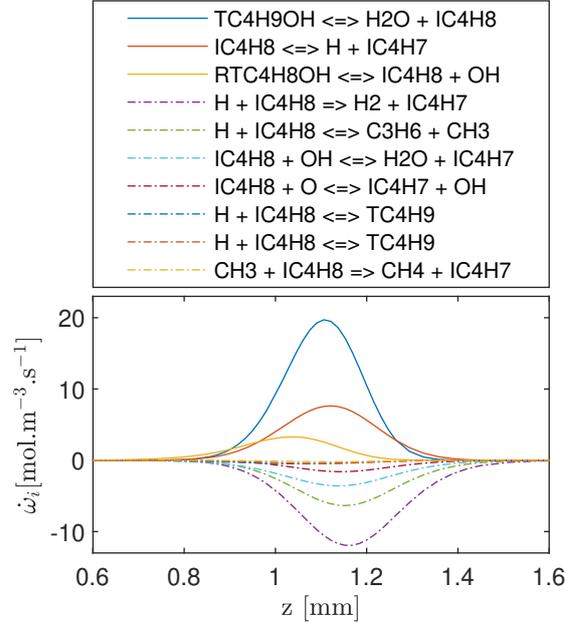


Figure 8: Partial production rates of $i$-butene for $t$-butanol flame with CRECK mechanism.

11

$$A_I^{prod} = \sum_{i=1}^{I} A_i^{prod} \qquad (10)$$

Finally, the contribution of the $i$th on the production of the species $n$ is deduced from:

$$c_i^{prod} = \frac{A_i^{prod}}{A_I^{prod}} \qquad (11)$$

In the previous example, dehydration reaction (R1) accounts for 59%, H-addition for 28% and $\beta$-scission (R2) for 11%. These reaction contributions are useful to understand the evolution of alkene levels of the different kinetic mechanisms.

Tab. 9 presents the production of butene isomers computed in butanol-doped flames. Only the cases where reactions R1 and R2 take place are reported (2-butene for 2-butanol, 1-butene for 1-,2-butanol and $i$-butene for $i$-, $t$-butanol).

Table 9: Reaction contribution (%) for the production of butene isomers by butanol isomers. Left columns : Sarathy; Right columns : CRECK.

| Reaction | 1-ol 1-ene | | $i$-ol $i$-ene | | 2-ol 1-ene | | 2-ol 2-ene | | $t$-ol $i$-ene | |
|---|---|---|---|---|---|---|---|---|---|---|
| dehyd. | 2 | 8 | 2 | 17 | 9 | 27 | 7 | 19 | 15 | 59 |
| $\beta$-scis. | 49 | 32 | 77 | 53 | 15 | 4 | 69 | 33 | 73 | 11 |
| H-add. | 13 | 0 | 11 | 28 | 23 | 0 | 23 | 17 | 11 | 28 |
| allyl + methyl | 29 | 55 | 0 | 0 | 43 | 62 | 0 | 0 | 0 | 0 |

Both mechanisms can be quite different concerning the butene isomers. For instance, dehydration reaction never accounts for more than 15% with Sarathy mechanism whereas it reaches 59% for CRECK mechanism in the case of $t$-butanol flame. On the other hand, $\beta$-scission reactions are the main pathways in many cases, with both mechanisms. Moreover, it worths noticing that there is no case where both mechanisms have similar pathways. It can be explained easily by the fact that for these reactions Arrhenius parameters (i.e. A and Ea) cover a rather large range of values. While the value of the activation energy in the case of dehydration of $t$-butanol seems to always be given around 65 kcal/mol, the other R1 and R2 reactions and associated Arrhenius constants vary more in the literature ([6, 16, 44, 22]. This underline the need of supplementary works to define the reaction rate of such reactions with a better accuracy.

### 4.5. Pentanol

There are 8 pentanol isomers, 4 primary alcohols, 3 secondary alcohols and 1 tertiary alcohol. This paper presents, to the author's knowledge, the first flame structure of a flame doped by 2,2-dimethyl-propanol, which is solid below 325 K. Important distinctions on average molar fractions can be noticed on $C_3H_6$, $C_3H_4$, $C_4H_6$, butene and pentene isomers (cf. Fig. 5). There is almost a factor 3 on propene level among the isomers, 3-methyl-2-butanol being maximum with an average of 270 ppm and 1- and $t$-pentanol minimum with 100 ppm.

Propadiene reaches its highest level with 2,2-dimethyl-propanol and $t$-pentanol (average of 25 ppm) then no major distinction can be given to the other isomers. Interestingly, similar trends are observed by butanol isomers: the $t$-butanol produced the most of propadiene, followed by the $i$-butanol (the branched primary alcohol).

Butadiene production varies also significantly, there is a factor 4 between 1-pentanol flame (minimum) and 3-pentanol flame (maximum).

Concerning the butene isomers, 1-butene is mostly produced by 3-pentanol (average of 56 ppm) and 2-butene by 3-methyl-2-butanol and 2-methyl-1-butanol. Finally, $i$-butene is produced at a significant level by 2,2-dimethyl-propanol flame (average of 200 ppm), then by $t$-pentanol, and almost not produced by linear isomers (less than 1 ppm). $i$-butene seems the most natural product from 2,2-dimethyl-propanol, since reaction R1 and R2 cannot happen, and the position of the maximum $i$-butene is indeed farther in the flame.

Pentene production by pentanol is represented in Fig. 9. Similarly to propanol and butanol isomers, for all cases (except 2,2-dimethyl-propanol), a link can be drawn between observed molar fractions and reactions R1 and R2.

1. 1-pentanol produces mainly 1-pentene,

2. 2-methyl-1-butanol produces mostly 2-methyl-1-butene (2 times higher than the other pentene isomers),

3. $i$-pentanol produces mostly 3-methyl-1-butene,

4. 2,2-dimethyl-propanol produces mostly 2-methyl-2-butene, and has the highest global level of pentenes among the primary alcohols,

5. 2-pentanol produces mostly 1- and 2-pentene,

6. 3-pentanol produces mostly 2-pentene (R1 and R2 forming exclusively 2-pentene by symmetry of the molecule),

7. 3-methyl-2-butanol produces mostly 3-methyl-1-butene and 2-methyl-2-butene but interestingly 2-methyl-1-butene as well, and the global level of pentenes is the highest among the secondary alcohols,
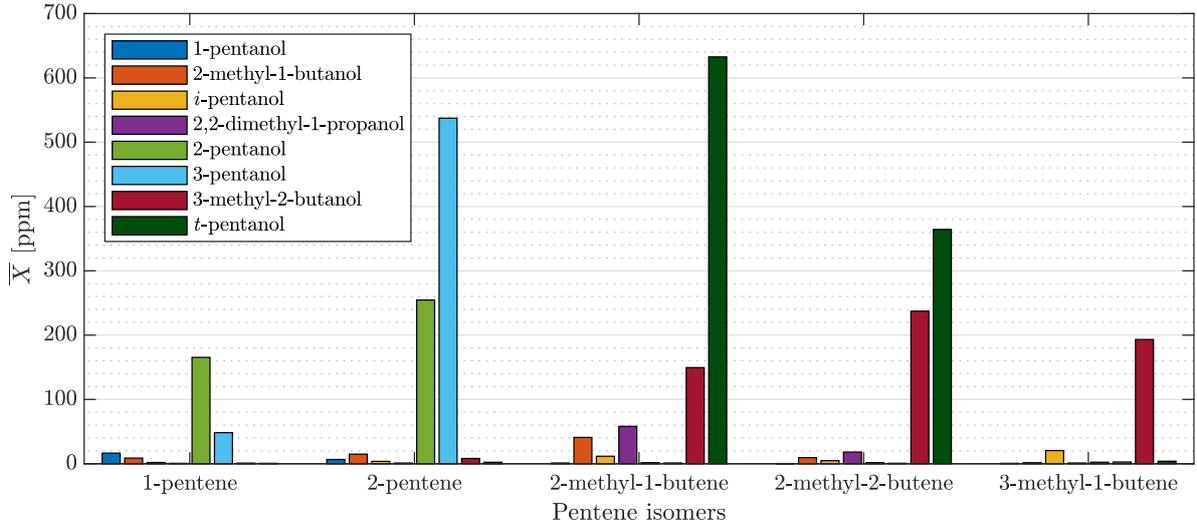
Figure 9: $\overline{X}$ of pentene isomers for pentanol flames.

8. $t$-pentanol produces mostly 2-methyl-1-butene and 2-methyl-2-butene (with almost a factor 2 between them, which could be expected by R1 and R2) and has the highest global level of pentenes among the 8 isomers.

The case of 2,2-dimethyl-propanol is interesting. Indeed, neither R1 or R2 can occur, because of the configuration of the molecule (double bonding impossible on the $\beta$ carbon). However, the most produced pentene isomers remain the ones with a methyl in position 2 (2-methyl-1-butene and 2-methyl-2-butene) and the position of the maximum is similar to the other pentanol cases.

The comparison between numerical and experimental results is more restrained because the kinetic mechanism used included only the three linear isomers of pentanol, i.e. 1-,2- and 3-pentanol. In this mechanism, 2 pentene isomers are included (1- and 2-pentene). As previously for propanol and butanol, the Köhler mechanism does predict the expected isomers of pentene for each isomer of pentanol but the level is much lower than experimental ones, especially for secondary alcohols.

### 4.6. Similar trends among all studied alcohols

As already mentioned, the four kinetic mechanisms used do not predict the level of alkenes produced by the different dopants. Experimentally, a clear hierarchy of alkene production level as a function of the type of alcohol has been established:

$$primary < secondary < tertiary.$$

To illustrate this statement, Fig. 10 presents the average molar fraction of propene for propanol flame, the sum of butene isomers average molar fractions for butanol-flames and the sum of pentene isomers average molar fractions for pentanol-flames as function of the type of alcohol. A factor 2.2 is observed between the lowest mean molar fraction from secondary alcohol and the highest level from primary alcohol, as well as a factor 1.7 between tertiary and secondary alcohols. A second feature can be extracted from Fig. 10: the branched fuels produce a higher level of alkenes than the linear ones, such as $i$-butanol compared to 1-butanol, or $i$-pentanol and 2-methyl-1-butanol compared to 1-pentanol.

Experimental results show that among all the intermediates only the alkene with the same number of carbons as the dopant has its maximum molar fraction at a very low $z$. This trend suggests a direct pathway from the dopant to the alkene. Moreover, the results obtained by measuring distinctly the 3 butene isomers and the 5 pentene isomers highlights that the products of R1 and R2 are always the major isomers (for the 13 dopants). For instance, 2-butanol produces effectively 1- and 2-butene, and 3-pentanol produces mostly 2-pentene. These reasons suggest the importance of these two types of reactions in the first steps of the alcohol decomposition. These reactions might occur for lower temperature than expected, i.e. below 900 K [4]. The results suggest also that, in alcohol-doped premixed rich flames of $C_2H_4$ ($\phi$=1.7), the alcohol could be degraded similarly than in diffusion flame. Indeed, the results are quite similar to Ref. [6] (nearly 75% of the tertiary alco-
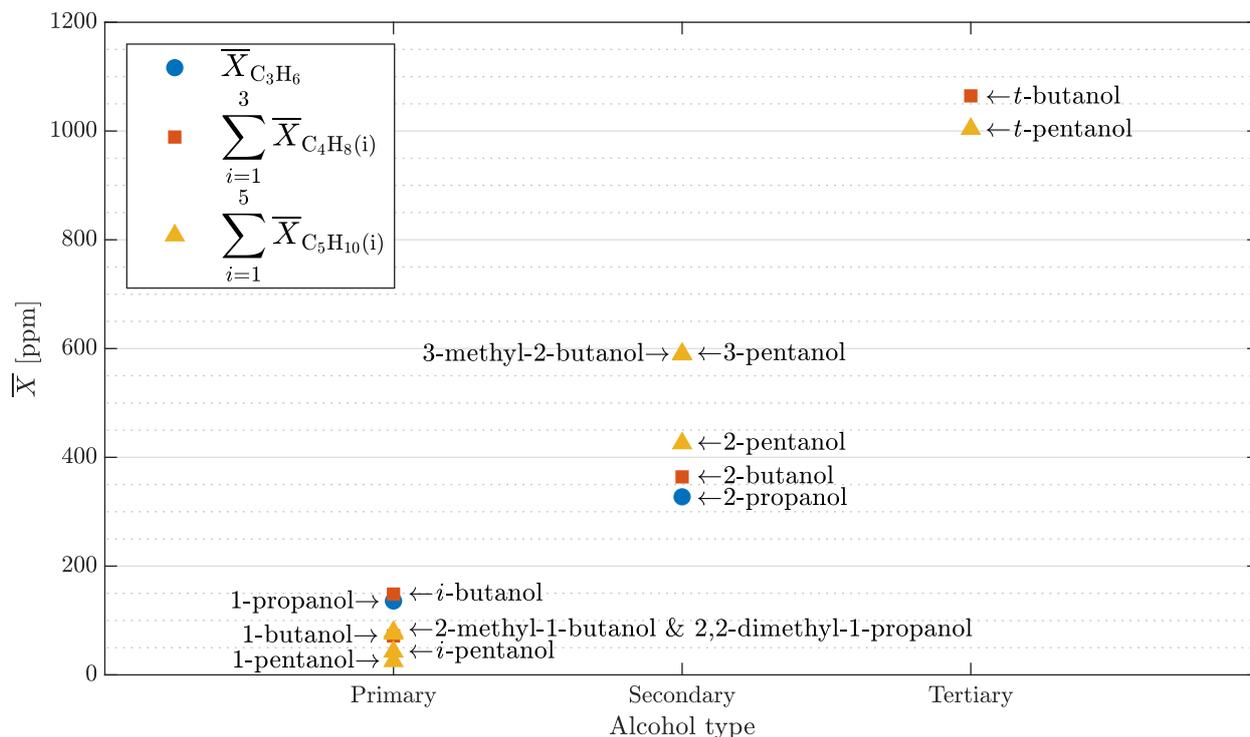
13

Figure 10: Comparison of alkenes production by type of alcohol (respectively propene, butene and pentene isomers for propanol, butanol and pentanol isomers).

hols might be converted in alkenes) and the numerical simulations performed in the present work indicate that $O_2$ and $O^\bullet$ are not involved in the alkene production.

On the other hand, numerical results do not reproduce (i) the peak location, (ii) the hierarchy among alcohol types, (iii) the hierarchy among linear and branched fuels, and mostly (iv) the amount of alkene produced (with a factor up to 20 for the case of butene produced by $t$-butanol in the simulation with Sarathy mechanism). With the lack of consensus among kinetic mechanisms regarding R1 and R2, the experimental database developed in the framework of this work shall be valuable for the validation of improved kinetic mechanisms. These improvements will allow a better prediction of alcohol conversion and, ultimately, could also lead to a better prediction of soot precursors.

## 5. Summary and conclusions

Fuel-rich, premixed atmospheric flames of ethylene doped by all the $C_3$ to $C_5$ alcohols were investigated by Gas Chromatography. 19 species have been identified and quantified, including the 3 butene isomers and the 5 pentene isomers. All flames exhibit similar macroscopic characteristics, such as major species profiles.

However intermediate species pool measured for the isomeric fuels differs strongly. Firstly, the alcohol type seems to play a role in the production of alkenes with the same number of carbon as the fuels. Primary alcohols produce the least alkenes while tertiary alcohols generate the most. With a lower order of magnitude, branched fuels seem to produce more alkene than linear ones.

Two types of reactions, R1 and R2 are suggested to explain most of the conversion from alcohol to alkene. Indeed for every fuel, products of these reactions are the alkenes presenting the highest molar fractions. It suggests that these reactions might occur under temperatures lower than currently predicted by the four kinetic mechanisms. These differences could play a role in soot formation and need to be confirmed on other configurations.

Considering the probable important role of R1 and R2, these experimental results could help to the development of kinetic mechanisms including alcohol fuels up to $C_5$, or eventually higher, since all $C_3$-$C_5$ alcohols seem to have similar behavior regarding alkene of the same number of carbons. These improvements could lead to a better prediction of alcohol combustion inter-

mediates and soot precursors, which ultimately would help to the modelization of soot emission.

Future works plan to study the same dopants in diffusion flames associated with optical diagnostics to measure soot characteristics such as volume fraction. The different alkene levels might lead to important discrepancies in sooting propensity among the different dopants.Then investigations should address the impact of pressure on the flames. Among others, Griffin et al. [45] showed that the sooting propensity of $C_2$-$C_4$ alkenes seems to increase significantly with pressure, this trend being more important for ethylene than propene or butene.

## References

[1] M. Lapuerta, O. Armas, J. M. Herreros, Fuel 87 (2008) 25–31.

[2] C. S. McEnally, L. D. Pfefferle, Environmental Science & Technology 45 (2011) 2498–2503.

[3] S. Kumar, J. H. Cho, J. Park, I. Moon, Renewable and Sustainable Energy Reviews 22 (2013) 46–72.

[4] S. M. Sarathy, P. Oßwald, N. Hansen, K. Kohse-Höinghaus, Progress in Energy and Combustion Science 44 (2014) 40–102.

[5] J. Abboud, J. Schobing, G. Legros, J. Bonnety, V. Tschamber, A. Brillard, G. Leyssens, V. Lauga, E. E. Iojoiu, P. Da Costa, Fuel 193 (2017) 241–253.

[6] C. S. McEnally, L. D. Pfefferle, Proceedings of the Combustion Institute 30 (2005) 1363–1370.

[7] P. Oßwald, H. Güldenberg, K. Kohse-Höinghaus, B. Yang, T. Yuan, F. Qi, Combustion and Flame 158 (2011) 2–15.

[8] M. Köhler, T. Kathrotia, P. Oßwald, M. L. Fischer-Tammer, K. Moshammer, U. Riedel, Combustion and Flame 162 (2015) 3197–3209.

[9] T. Walther, J. M. François, Biotechnology Advances 34 (2016) 984–996.

[10] S. P. H. Azambuja, R. Goldbeck, World Journal of Microbiology and Biotechnology 36 (2020) 48.

[11] A. F. Cann, J. C. Liao, Applied Microbiology and Biotechnology 85 (2010) 893–899.

[12] M. R. Connor, J. C. Liao, Current Opinion in Biotechnology 20 (2009) 307–315.

[13] Y. Li, L. Wei, Z. Tian, B. Yang, J. Wang, T. Zhang, F. Qi, Combustion and Flame 152 (2008) 336–359.

[14] T. Kasper, P. Oßwald, U. Struckmeier, K. Kohse-Höinghaus, C. A. Taatjes, J. Wang, T. A. Cool, M. E. Law, A. Morel, P. R. Westmoreland, Combustion and Flame 156 (2009) 1181–1201.

[15] A. Frassoldati, A. Cuoci, T. Faravelli, U. Niemann, E. Ranzi, R. Seiser, K. Seshadri, Combustion and Flame 157 (2010) 2–16.

[16] R. Grana, A. Frassoldati, T. Faravelli, U. Niemann, E. Ranzi, R. Seiser, R. Cattolica, K. Seshadri, Combustion and Flame 157 (2010) 2137–2154.

[17] X. Man, C. Tang, J. Zhang, Y. Zhang, L. Pan, Z. Huang, C. K. Law, Combustion and Flame 161 (2014) 644–656.

[18] W. Li, Y. Zhang, B. Mei, Y. Li, C. Cao, J. Zou, J. Yang, Z. Cheng, Combustion and Flame 207 (2019) 171–185.

[19] G. Capriolo, A. A. Konnov, Combustion and Flame 218 (2020) 189–204.

[20] J. T. Moss, A. M. Berkowitz, M. A. Oehlschlaeger, J. Biet, V. Warth, P.-A. Glaude, F. Battin-Leclerc, The Journal of Physical Chemistry A 112 (2008) 10843–10855. Publisher: American Chemical Society.

[21] X. Gu, Z. Huang, S. Wu, Q. Li, Combustion and Flame 157 (2010) 2318–2325.

[22] A. Frassoldati, R. Grana, T. Faravelli, E. Ranzi, P. Oßwald, K. Kohse-Höinghaus, Combustion and Flame 159 (2012) 2295–2311.

[23] F. Wu, C. K. Law, Combustion and Flame 160 (2013) 2744–2756.

[24] P. Singh, X. Hui, C.-J. Sung, Combustion and Flame 164 (2016) 167–182.

[25] C. Russo, A. D'Anna, A. Ciajolo, M. Sirignano, Combustion and Flame 199 (2019) 122–130.

[26] G. Dayma, C. Togbé, P. Dagaut, Energy & Fuels 25 (2011) 4986–4998.

[27] C. Togbé, F. Halter, F. Foucher, C. Mounaim-Rousselle, P. Dagaut, Proceedings of the Combustion Institute 33 (2011) 367–374.

[28] K. A. Heufer, S. M. Sarathy, H. J. Curran, A. C. Davis, C. K. Westbrook, W. J. Pitz, Energy & Fuels 26 (2012) 6678–6685.

[29] S. Mani Sarathy, S. Park, B. W. Weber, W. Wang, P. S. Veloo, A. C. Davis, C. Togbe, C. K. Westbrook, O. Park, G. Dayma, Z. Luo, M. A. Oehlschlaeger, F. N. Egolfopoulos, T. Lu, W. J. Pitz, C.-J. Sung, P. Dagaut, Combustion and Flame 160 (2013) 2712–2728.

[30] S. Park, O. Mannaa, F. Khaled, R. Bougacha, M. S. Mansour, A. Farooq, S. H. Chung, S. M. Sarathy, Combustion and Flame 162 (2015) 2166–2176.

[31] Q. Li, C. Tang, Y. Cheng, L. Guan, Z. Huang, Energy & Fuels 29 (2015) 5334–5348.

[32] Q. Li, E. Hu, X. Zhang, Y. Cheng, Z. Huang, Energy & Fuels 27 (2013) 1141–1150.

[33] C. Tang, L. Wei, X. Man, J. Zhang, Z. Huang, C. K. Law, Combustion and Flame 160 (2013) 520–529.

[34] M. Kashif, P. Guibert, J. Bonnety, G. Legros, Combustion and Flame 161 (2014) 1575–1586.

[35] Y. Wang, S. Park, S. M. Sarathy, S. H. Chung, Combustion and Flame 192 (2018) 71–85.

[36] Y. Ying, D. Liu, Fuel 205 (2017) 109–129.

[37] C. S. McEnally, L. D. Pfefferle, Combustion and Flame 148 (2007) 210–222.

[38] J. Abboud, Impact des suies issues de biocarburants sur le filtre à particules, PhD, Sorbonne Université, 2018.

[39] S. S. Yang, L. Gülder, Combustion and Flame 220 (2020) 203–209.

[40] A. Tipler, PerkinElmer Application Note (2010).

[41] D. G. Goodwin, H. K. Moffat, R. L. Speth, Cantera: An Object-Oriented Software Toolkit For Chemical Kinetics, Thermodynamics, And Transport Processes. Version 2.3.0, 2017.

[42] W. H. Green, J. W. Allen, B. A. Buesser, R. W. Aschraft, G. J. Beran, C. A. Class, C. Gao, C. F. Goldsmith, M. R. Harper, A. Jalan, M. Keceli, G. R. Magoon, D. M. Matheu, S. S. Merchant, J. D. Mo, S. Petway, S. Raman, S. Sharma, J. Song, Y. Suleymanov, K. M. Van Geem, J. Wen, R. H. West, A. Wong, P. E. Yelvington, N. Yee, J. Yu, RMG - Reaction Mechanism Generator v4.0.1, 2013.

[43] H. Wang, M. Frenklach, The Journal of Physical Chemistry 98 (1994) 11465–11489. Publisher: American Chemical Society.

[44] S. M. Sarathy, S. Vranckx, K. Yasunaga, M. Mehl, P. Oßwald, W. K. Metcalfe, C. K. Westbrook, W. J. Pitz, K. Kohse-Höinghaus, R. X. Fernandes, H. J. Curran, Combustion and Flame 159 (2012) 2028–2055.

[45] E. A. Griffin, L. Gülder, Combustion and Flame 197 (2018) 378–388.